


# Origin of the intermediate-temperature magnetic specific heat capacity in the spin-liquid candidate $\text{Ca}_{10}\text{Cr}_7\text{O}_{28}$

Joe Crossley <sup>\*</sup>

SUPA, School of Physics and Astronomy, University of St Andrews, North Haugh, St Andrews, Fife KY16 9SS, United Kingdom

Chris Hooley <sup>†</sup>

Max Planck Institute for the Physics of Complex Systems, Nöthnitzer Straße 38, 01187 Dresden, Germany



(Received 24 November 2023; accepted 21 March 2024; published 19 April 2024)

We present several approximate calculations of the specific heat capacity of the model for  $\text{Ca}_{10}\text{Cr}_7\text{O}_{28}$  proposed by Balz *et al.* [*Phys. Rev. B* **95**, 174414 (2017)], using methods including exact diagonalization, thermal pure quantum states, and high-temperature expansions. In none of these cases are we able to reproduce the magnitude of the zero-field specific heat capacity shown in the intermediate-temperature ( $\sim 5\text{--}15\text{ K}$ ) experimental data. We discuss possible reasons for the discrepancy, and what it might tell us about the magnetic Hamiltonian for  $\text{Ca}_{10}\text{Cr}_7\text{O}_{28}$ .

DOI: [10.1103/PhysRevB.109.165138](https://doi.org/10.1103/PhysRevB.109.165138)

## I. INTRODUCTION

This year marks the 50th anniversary of Anderson’s famous suggestion [1] that the ground state of the spin-1/2 Heisenberg model on the triangular lattice might be a resonating valence bond state. Despite the now convincing evidence that the ground state of that particular model has Néel order [2–4], Anderson’s proposal—together with the discovery 13 years later of the high- $T_c$  cuprate family of materials [5,6]—provoked an interest in the study of so-called “spin-liquid” phases which persists to this day [7,8].

One candidate spin-liquid material that has given rise to considerable interest over the past few years is  $\text{Ca}_{10}\text{Cr}_7\text{O}_{28}$ . Balz *et al.* have suggested a two-dimensional (2D) model [9–12], while Alshalawi *et al.* recently proposed a three-dimensional (3D) description [13]. Both of these sets of authors attribute the magnetic behavior of  $\text{Ca}_{10}\text{Cr}_7\text{O}_{28}$  to the six  $\text{Cr}^{5+}$  ions in each formula unit [10]. These are arranged in distorted kagome planes, with each site hosting a well-localized spin-1/2 degree of freedom.

The model proposed by Balz *et al.* is known as the breathing bilayer kagome (BBK) Hamiltonian,

$$\hat{H} = \sum_{\langle i,j \rangle} J_{ij} \hat{\mathbf{S}}_i \cdot \hat{\mathbf{S}}_j - g\mu_B h \sum_i \hat{S}_i^z, \quad (1)$$

where  $\langle i, j \rangle$  denotes summation over nearest-neighbor bonds (counting each bond only once),  $h$  denotes the applied

magnetic field strength, and the  $g$  factor is taken to be 2. This 2D model couples kagome layers into bilayers as shown in Fig. 1. The term “breathing” refers to the inequivalence of the differently oriented triangles within each kagome plane. The couplings themselves are of weak Heisenberg type, and have a mixed ferro-/antiferromagnetic nature. Their numerical values, given by Balz *et al.*, are included in Fig. 1; Balz *et al.* determined these by fitting the structure factor of the model to the spin-wave spectrum of  $\text{Ca}_{10}\text{Cr}_7\text{O}_{28}$  under a high magnetic field.

There is good reason to believe that both the model (BBK) and the corresponding material ( $\text{Ca}_{10}\text{Cr}_7\text{O}_{28}$ ) exhibit spin-liquid behavior at the lowest temperatures [9,11,12,14–18]. The purpose of this paper is not to question those beliefs, but rather to present evidence that the BBK model is appreciably incomplete as a description of the magnetism of  $\text{Ca}_{10}\text{Cr}_7\text{O}_{28}$ . We are not the first to raise concerns along these lines; Pohle *et al.* [14] noted that the presence of finite-energy scattering weight at  $\mathbf{q} = \mathbf{0}$  in zero-field neutron scattering experiments implies that there is significant anisotropy in the exchange interactions, a feature that the model (1) does not reproduce. In this paper we further test this model by using various methods to calculate its specific heat capacity (with and without a 12 T field); we shall focus especially on the zero-field specific heat capacity because it is here that the inconsistency between the model and experiment is most clearly seen. Balz *et al.* also discuss, though ultimately discard, an alternative model called the “coupled hexagon model” [10]. This model, too, appears unable to reproduce the specific heat capacity of  $\text{Ca}_{10}\text{Cr}_7\text{O}_{28}$  (results presented in Supplemental Material [19]).

The remainder of this paper is structured as follows. In Sec. II, we present the results of four different methods used to approximately calculate the specific heat capacity of the BBK model: the strong-triangle approximation (an approach based on the hierarchy of coupling strengths), exact diagonalization, thermal pure quantum states, and the high-temperature

<sup>\*</sup>Corresponding author: [jc413@st-andrews.ac.uk](mailto:jc413@st-andrews.ac.uk)<sup>†</sup>[hooley@pks.mpg.de](mailto:hooley@pks.mpg.de)

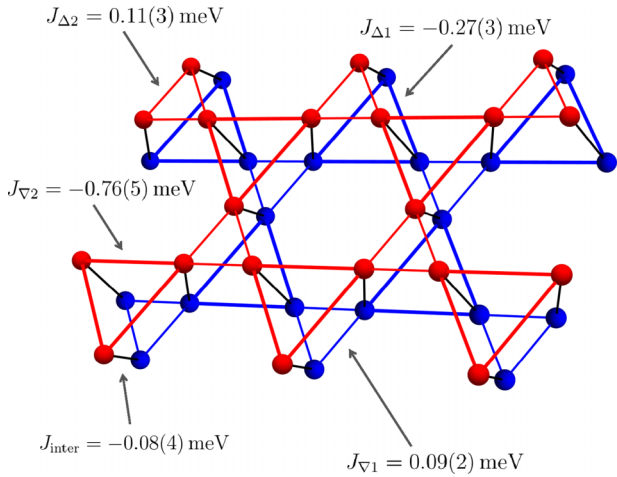


FIG. 1. A section from a single bilayer of  $\text{Ca}_{10}\text{Cr}_7\text{O}_{28}$ . The blue and red spheres denote  $\text{Cr}^{5+}$  ions from layers 1 and 2, respectively. All distinct couplings in the breathing bilayer kagome model are indicated by their symbol and associated value, as determined by Balz *et al.* in Ref. [11].

expansion. In Sec. III we discuss our results, and the modifications to the magnetic model of  $\text{Ca}_{10}\text{Cr}_7\text{O}_{28}$  that they might suggest.

## II. RESULTS

### A. Strong-triangle approximation

We expect something of a separation of scales in the BBK model since the  $J_{\Delta 1}$  and  $J_{\nabla 2}$  couplings stand out as stronger than the rest. This allows one to calculate the dominant contribution to the high-temperature specific heat capacity by switching off all other couplings, leaving isolated “strong triangles.” The unit cell of the bilayer lattice contains exactly one of each of the two types of strong triangle. These unit cells are noninteracting in this approximation and thus the specific heat capacity of the whole structure can be inferred from the partition function of a single unit cell,

$$\mathcal{Z}_{\text{cell}}(\beta) = \left( \sum_i e^{-\beta \epsilon_i^{\Delta 1}(h)} \right) \left( \sum_j e^{-\beta \epsilon_j^{\nabla 2}(h)} \right), \quad (2)$$

where  $\epsilon_i^{\Delta 1}(h)$  and  $\epsilon_j^{\nabla 2}(h)$  are the energy levels of each of the two types of triangle, calculated by diagonalizing the relevant  $8 \times 8$  matrix obtained from (1).

We show our results in Fig. 2 for the 0 and 12 T specific heat capacities calculated using this technique. Clearly the approximation works fairly well in the presence of a 12 T field. We expect this to be the case as the gap between eigenstates is well accounted for by the Zeeman and stronger ferromagnetic terms alone. In the absence of any external field, on the other hand, gaps between the lowest-energy eigenstates occur only if we include the weaker bonds. Thus, our strong-triangle approximation cannot correctly reproduce the zero-field specific heat capacity at the lowest temperatures. This is no surprise; more concerning, however, it shows significant disagreement with the experimental data even in the intermediate-temperature range (5–15 K). Could this be

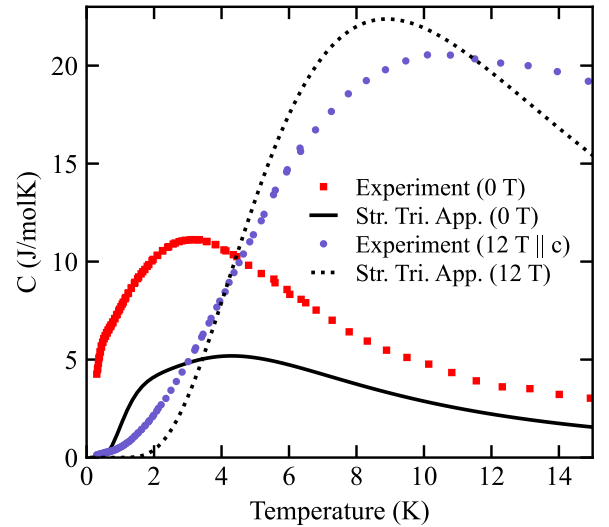


FIG. 2. The specific heat capacity of the breathing bilayer kagome model (1) using the strong-triangle approximation, in zero magnetic field (solid black curve) and in a magnetic field of 12 T (dotted black curve). Experimental data, previously published in Ref. [11], are also shown for comparison.

due purely to the omission of the weaker exchange couplings, or must other physics be invoked to account for it?

### B. Exact diagonalization

In an initial attempt to recover something of the weak-coupling physics we now “switch on”  $J_{\nabla 1}$  and  $J_{\Delta 2}$ , neglecting only  $J_{\text{inter}}$ . This enables a simple exact diagonalization description where one diagonalizes a cluster of spins in each layer and then combines their spectra to calculate the specific heat capacity (see Supplemental Material [19] for cluster dimensions). The calculation ends up looking much as that of the first technique,

$$\mathcal{Z}_{\text{cluster}}(\beta) = \left( \sum_i e^{-\beta \epsilon_i^1(h)} \right) \left( \sum_j e^{-\beta \epsilon_j^2(h)} \right), \quad (3)$$

the difference being that the energy levels  $\epsilon_i^1(h)$  and  $\epsilon_j^2(h)$  are found by diagonalizing (1) for not 3 but 12 spins in layers 1 and 2, respectively.

We show our results for a cluster of 24 spins in Fig. 3. Comparison with Fig. 2 confirms that the inclusion of  $J_{\nabla 1}$  and  $J_{\Delta 2}$  causes no significant change to the 12 T curve. The story is somewhat similar for the zero-field curve, which appears to exactly follow that of the strong-triangle approximation down to  $\sim 4$  K, and still falls far short of the experimental specific heat capacity across almost the entire measured temperature range. We now turn to two more powerful techniques where all couplings are properly accounted for.

### C. Thermal pure quantum states

The method of canonical thermal pure quantum states (TPQS) was introduced by Sugiura and Shimizu [20]. Fundamentally approximate, it can be used as an alternative to exact diagonalization, enabling larger cluster sizes to be treated.

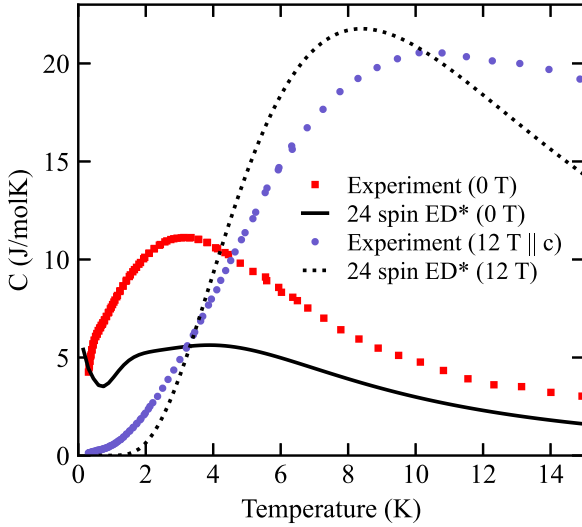


FIG. 3. The specific heat capacity of the breathing bilayer kagome model (1) calculated using exact diagonalization of a cluster of 24 spins (12 per layer), in zero magnetic field (solid black curve) and in a magnetic field of 12 T (dotted black curve). “ED\*” denotes that the exact diagonalization was performed with  $J_{\text{inter}} = 0$ . Experimental data, previously published in Ref. [11], are shown for comparison.

The method works by selecting a random vector  $|\psi_0\rangle$  in the many-body Hilbert space and using this pure state as a kind of proxy for the true infinite-temperature mixed state. This “thermal state” is cooled down step by step as follows,

$$|k\rangle = (l - \hat{h})|k-1\rangle = (l - \hat{h})^k |\psi_0\rangle, \quad (4)$$

where  $\hat{h} = \hat{H}/N$ ,  $N$  is the number of lattice sites, and  $l$  is an upper bound on the eigenvalue spectrum of  $\hat{h}$ . By taking expectation values at each iteration, thermodynamic variables can be calculated as functions of temperature. In our case, we found the heat capacity from the numerical temperature derivative of the energy per particle,

$$\langle \hat{h} \rangle_{\beta, N} \approx \sum_{k=0}^{\infty} (N\beta)^{2k} \left( \frac{\langle k | \hat{h} | k \rangle}{(2k)!} + N\beta \frac{\langle k | \hat{h} | k+1 \rangle}{(2k+1)!} \right), \quad (5)$$

which we evaluated to sufficiently high order that the associated truncation error may reasonably be ignored compared to the uncertainty due to the initial starting state. Sugiura and Shimizu provide a method for estimating this latter uncertainty. We followed their scheme and ensured that the uncertainty margin on all our results never exceeded  $\sim 1\%$ . We also benchmarked our code against the data of Elstner and Young for the spin-1/2 Heisenberg antiferromagnet on the kagome lattice [21] (see Supplemental Material [19]).

Figure 4 shows the zero-field TPQS specific heat capacity of (1) for clusters of 18, 24, and 30 spins (see Supplemental Material [19] for exact cluster dimensions). The TPQS method becomes more accurate for larger Hilbert spaces. In the 30-spin case a single TPQS run was sufficient but for smaller clusters we averaged our results over several runs to bring our uncertainty measures down: eight runs for the 24-spin case and 100 runs for the 18-spin case. Our results were obtained by parallelizing the calculation across 64 cores

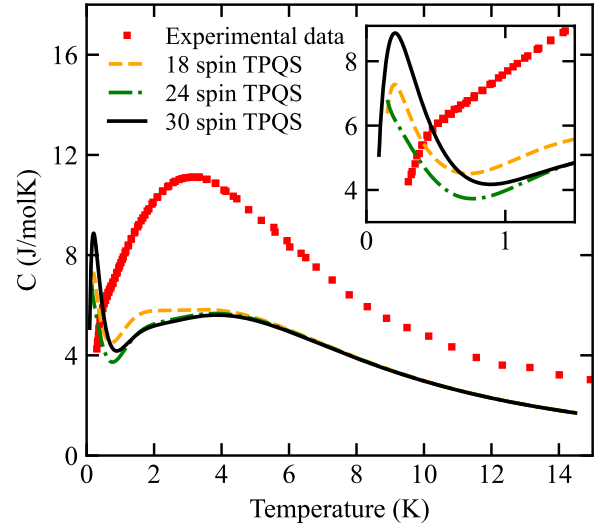


FIG. 4. The specific heat capacity of the breathing bilayer kagome model (1) calculated using thermal pure quantum states for clusters of 18, 24, and 30 spins, in the absence of a magnetic field. For 18 spins we averaged across 100 runs, for 24 spins we averaged across eight runs, and for 30 spins only a single run was used. In all cases the uncertainty margin at each temperature never exceeds  $\sim 1\%$ . The experimental zero-field specific heat capacity of  $\text{Ca}_{10}\text{Cr}_7\text{O}_{28}$ , previously published in Ref. [11], is also shown. For clarity, we have included an inset which enlarges the heat capacity curves at the lowest temperatures.

of one of the nodes in the Edinburgh Sun Grid Engine cluster. Due to memory considerations, we successively generated the matrix elements of the Hamiltonian rather than storing them all simultaneously.

For spin clusters of these sizes, the separation of coupling strengths in the model (1) is clearly manifest in the two distinct peaks in the specific heat capacity. No such double-peak structure is seen in the experimental data.

#### D. High-temperature expansion

The high-temperature expansion (HTE) expresses the partition function as

$$\mathcal{Z}(\beta) = \text{Tr}[\mathbb{1}] - \beta \text{Tr}[\hat{H}] + \frac{\beta^2}{2} \text{Tr}[\hat{H}^2] - \frac{\beta^3}{3!} \text{Tr}[\hat{H}^3] + \dots \quad (6)$$

For spin systems, the expansion coefficients decompose into much smaller traces over products of spin-spin bonds appearing in the Hamiltonian. However, these “moments” become increasingly complex for higher orders.

Following Ref. [22], we calculated the first five moments for the heat capacity of (1) by hand. The C++ package by Lohmann *et al.* [23] enabled us to further calculate the series up to tenth order, as well as providing three different Padé approximants to extend the series. The package only allows for four different coupling strengths, so we set  $J_{\nabla_1} = J_{\Delta_2}$  (which is in any case consistent with the quoted uncertainties in these coupling constants) in these cases.

We show our results in Fig. 5 along with the experimental zero-field specific heat capacity and the 30-spin TPQS curve

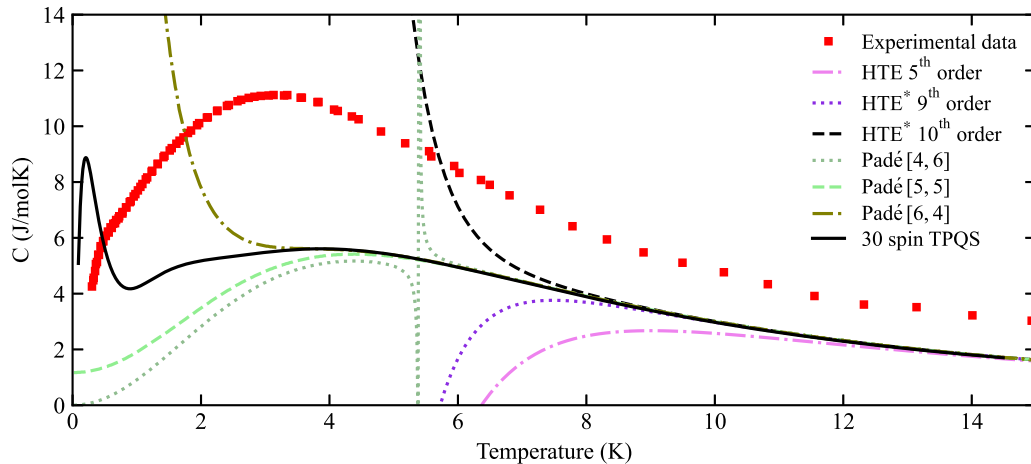


FIG. 5. The specific heat capacity of the breathing bilayer kagome model (1) in the absence of a magnetic field, calculated using the high-temperature expansion to various orders as stated in the legend. The curves labeled “HTE\*” were calculated using a software package [23] allowing only four different coupling strengths, so we set  $J_{\nabla 1} = J_{\Delta 2}$  in these cases (which is in any case consistent with the quoted uncertainties in these coupling constants). The various Padé curves were also computed using the aforementioned software package; they are based on the tenth-order expansion obtained by the software, labeled here as “HTE\* 10th order.” For comparison, we show our 30-spin thermal pure quantum states curve for the model, as well as the experimental zero-field specific heat capacity data previously published in Ref. [11].

for comparison. Our finite-order results diverge at low temperatures as is normal for such series. Assuming further orders in the expansion are well behaved, one typically decides the temperature down to which such curves can be trusted by looking for the point at which consecutive orders separate appreciably from one another. The geometry of the BBK lattice gives no specific reason to expect the higher-order terms to be poorly behaved, so we take the ninth- or tenth-order curves as essentially correct down to  $\sim 9$  K.

The three Padé approximants agree down to even lower temperatures. These approximants are quotients of polynomials in  $J/(k_B T)$  and we label them Padé  $[L, M]$ , where  $L$  is the polynomial order of the numerator and  $M$  is the polynomial order of the denominator. A “complete” approximation to the heat capacity should converge to zero as  $T \rightarrow 0$ ; this is only guaranteed for approximants where  $L < M$  [21]. Yet, our curve for which this condition is satisfied (Padé  $[4,6]$ ) exhibits a dramatic singularity at intermediate temperatures. Comparison with the other approximants, as well as with the TPQS curve, suggests that this is a “spurious pole” (a well-known effect where the Padé approximant exhibits a pole that is not a feature of the target function). In any case, we find the three approximants in good agreement with one another right down to  $\sim 6$  K.

### III. DISCUSSION

All this has little to say to those interested in the spin-liquid phase of the BBK model; no method used in this study is expected to work well at such low temperatures. However, our calculations have clear implications for those who would use the model to describe the spin-liquid phase of  $\text{Ca}_{10}\text{Cr}_7\text{O}_{28}$ : If the model does not describe the material’s magnetism well at these intermediate temperatures, why should we expect it to perform well at the lowest temperatures?

The strong-triangle approximation is clearly a drastic one, especially in the absence of a magnetic field. Even so, it is very

useful: The one who believes that  $\text{Ca}_{10}\text{Cr}_7\text{O}_{28}$  is described by the BBK model (1) is forced to say that the weak couplings would, were they included, account for the difference between the calculated and measured specific heat capacities of Fig. 2. This requires that the weak couplings strongly enhance the specific heat capacity far beyond their temperature scale of  $\sim 1$  K, which intuitively seems unlikely given the structure of the model. To test this intuition we undertook three further calculations, all of which sought to include the effect of the weaker couplings.

Our exact diagonalization method includes all but one of the weaker-coupling types, and the TPQS method includes them all. As expected, these weaker couplings lead to no noticeable change in the specific heat capacity right down to  $\sim 4$  K; rather, a second peak emerges below 1 K, increasing the apparent disparity between theory and experiment. Yet both methods are subject to finite-size effects. We might question whether longer-range physics would push this new low-temperature peak upward to supplement the broader peak at  $\sim 4$  K—from an entropic perspective, this peak-migration effect could account for the difference between theory and experiment (see Supplemental Material [19]).

To address the issue of potential finite-size effects we now turn to our final technique, the high-temperature expansion, which allows us to calculate the specific heat capacity in the thermodynamic limit. The ninth- and tenth-order HTEs follow our 30-spin TPQS curve down to  $\sim 9$  K (below which we argue they are no longer valid anyway), and all the Padé extensions follow our 30-spin TPQS curve down to  $\sim 6$  K. Thus, despite finite-size effects, we claim that the 30-spin TPQS curve suitably reproduces the specific heat capacity of the BBK model (1) in the thermodynamic limit, right down to  $\sim 6$  K.

We are left with an apparent disparity between theory and experiment; what are we to make of it? One might seek a resolution by claiming that there remains a residual phononic contribution in the experimental data. The size of the



discrepancy, and the fact that it appears to be strongly dependent on the applied magnetic field, make it unlikely that this is the full story.

Another possibility is that the BBK model (1) is correct in spirit, but that the exact values of the five different isotropic couplings require further optimization in order to reproduce not only the 11 T neutron scattering data of  $\text{Ca}_{10}\text{Cr}_7\text{O}_{28}$  but also the specific heat capacity data. To explore this possibility fully would require a thorough variational search across the five-dimensional parameter space of the BBK model. Such an investigation is beyond the scope of this paper. However, as a test we can attempt to reverse the order of the procedure for determining the coupling constants. Balz *et al.* fitted the coupling constants to the single-spin-flip dispersion relations obtained via high-field inelastic neutron scattering; as we have shown, the resulting coupling constants do not account for the zero-field specific heat capacity. We have instead determined several sets of possible coupling constants via a fit to the high-temperature tail of the 0 T specific heat capacity, but in none of these cases do we find a reasonable fit to the single-spin-flip dispersion relations (see Supplemental Material [19]). Taking these results together with Pohle *et al.*'s argument for anisotropy in the exchange interactions (finite-energy scattering weight at  $\mathbf{q} = \mathbf{0}$ ) [14], we tentatively conclude that there is unlikely to be a pure Heisenberg model that reproduces all of the currently available experimental data on  $\text{Ca}_{10}\text{Cr}_7\text{O}_{28}$ .

A weak Dzyaloshinskii-Moriya interaction [14,17,24] would break the degeneracy of the ground state manifold of each of the strong triangles, leaving only a Kramers doublet in its place. This could be the mechanism by which the entropy under the low-temperature peak is moved to supplement the broader peak at higher temperatures. While such anisotropic interactions are not usually essential to describe the magnetism of 3d transition metal ions, the quoted strengths of the

Heisenberg interactions in the BBK model are themselves so weak that lower-symmetry effects need not be that great before they become important. One might oppose the suggestion of anisotropy by pointing to the similarity of the magnetic susceptibility curves of Balz *et al.* [11] when the field is applied along different crystal axis directions. However, local anisotropic effects in competition can conspire to produce exactly such behavior [25].

Alongside microscopic calculations based on a tight-binding expansion, we are currently exploring a variational approach based on the addition of general anisotropic exchange terms to the strong-triangle approximation, fitting to the wealth of experimental data available. While our plan is initially to focus on the strong bonds in the model, we hope this will also function to improve the accuracy of the model down to the lowest temperatures [25].

## ACKNOWLEDGMENTS

The authors would like to thank C. Balz, B. Lake, and N. Shannon for helpful discussions, and C. Balz and B. Lake for kindly sharing the original specific heat capacity and inelastic neutron scattering data published in Ref. [11]. We also thank A. Lohmann, J. Richter, and H.-J. Schmidt for their excellent C++ package for computing high-temperature expansions [23], which can be found online [28]. All thermal pure quantum states calculations were performed on the Edinburgh University SGE cluster. J.C. acknowledges support from UKRI via EPSRC Grant No. EP/T518062/1. C.H. acknowledges support from UKRI via EPSRC Grant No. EP/R031924/1. This work was performed in part at Aspen Center for Physics, which is supported by National Science Foundation Grant No. PHY-2210452.

- 
- [1] P. W. Anderson, Resonating valence bonds: A new kind of insulator? *Mater. Res. Bull.* **8**, 153 (1973).
  - [2] T. Jolicoeur and J. C. Le Guillou, Spin-wave results for the triangular Heisenberg antiferromagnet, *Phys. Rev. B* **40**, 2727(R) (1989).
  - [3] B. Bernu, P. Lecheminant, C. Lhuillier, and L. Pierre, Exact spectra, spin susceptibilities, and order parameter of the quantum Heisenberg antiferromagnet on the triangular lattice, *Phys. Rev. B* **50**, 10048 (1994).
  - [4] L. Capriotti, A. E. Trumper, and S. Sorella, Long-range Néel order in the triangular Heisenberg model, *Phys. Rev. Lett.* **82**, 3899 (1999).
  - [5] J. G. Bednorz and K. A. Müller, Possible high  $T_c$  superconductivity in the Ba-La-Cu-O system, *Z. Phys. B* **64**, 189 (1986).
  - [6] M.-K. Wu, J. R. Ashburn, C. J. Torng, P.-H. Hor, R. L. Meng, L. Gao, Z. J. Huang, Y. Q. Wang, and C. W. Chu, Superconductivity at 93 K in a new mixed-phase Y-Ba-Cu-O compound system at ambient pressure, *Phys. Rev. Lett.* **58**, 908 (1987).
  - [7] L. Savary and L. Balents, Quantum spin liquids: a review, *Rep. Prog. Phys.* **80**, 016502 (2017).
  - [8] C. Broholm, R. J. Cava, S. A. Kivelson, D. G. Nocera, M. R. Norman, and T. Senthil, Quantum spin liquids, *Science* **367**, eaay0668 (2020).
  - [9] C. Balz, B. Lake, J. Reuther, H. Luetkens, R. Schönemann, T. Herrmannsdörfer, Y. Singh, A. T. M. Nazmul Islam, E. M. Wheeler, J. A. R.-Rivera *et al.*, Physical realization of a quantum spin liquid based on a complex frustration mechanism, *Nat. Phys.* **12**, 942 (2016).
  - [10] C. Balz, B. Lake, M. Reehuis, A. T. M. Nazmul Islam, O. Prokhnenko, Y. Singh, P. Pattison, and S. Tóth, Crystal growth, structure and magnetic properties of  $\text{Ca}_{10}\text{Cr}_7\text{O}_{28}$ , *J. Phys.: Condens. Matter* **29**, 225802 (2017).
  - [11] C. Balz, B. Lake, A. T. M. Nazmul Islam, Y. Singh, J. A. Rodriguez-Rivera, T. Guidi, E. M. Wheeler, G. G. Simeoni, and H. Ryll, Magnetic Hamiltonian and phase diagram of the quantum spin liquid  $\text{Ca}_{10}\text{Cr}_7\text{O}_{28}$ , *Phys. Rev. B* **95**, 174414 (2017).
  - [12] J. Sonnenschein, C. Balz, U. Tutsch, M. Lang, H. Ryll, J. A. Rodriguez-Rivera, A. T. M. Nazmul Islam, B. Lake, and J. Reuther, Signatures for spinons in the quantum spin liquid candidate  $\text{Ca}_{10}\text{Cr}_7\text{O}_{28}$ , *Phys. Rev. B* **100**, 174428 (2019).
  - [13] D. R. Alshalawi, J. M. Alonso, A. R. Landa-Cánovas, and P. de la Presa, Coexistence of two spin frustration pathways in the quantum spin liquid  $\text{Ca}_{10}\text{Cr}_7\text{O}_{28}$ , *Inorg. Chem.* **61**, 16228 (2022).

- [14] R. Pohle, H. Yan, and N. Shannon, Theory of  $\text{Ca}_{10}\text{Cr}_7\text{O}_{28}$  as a bilayer breathing-kagome magnet: Classical thermodynamics and semiclassical dynamics, *Phys. Rev. B* **104**, 024426 (2021).
- [15] A. Kshetrimayum, C. Balz, B. Lake, and J. Eisert, Tensor network investigation of the double layer Kagome compound  $\text{Ca}_{10}\text{Cr}_7\text{O}_{28}$ , *Ann. Phys.* **421**, 168292 (2020).
- [16] S. Biswas and K. Damle, Semiclassical theory for liquidlike behavior of the frustrated magnet  $\text{Ca}_{10}\text{Cr}_7\text{O}_{28}$ , *Phys. Rev. B* **97**, 115102 (2018).
- [17] P. Schmoll, C. Balz, B. Lake, J. Eisert, and A. Kshetrimayum, Finite temperature tensor network algorithm for frustrated two-dimensional quantum materials, [arXiv:2211.00121](https://arxiv.org/abs/2211.00121).
- [18] A. Balodhi and Y. Singh, Synthesis and pressure and field-dependent magnetic properties of the kagome-bilayer spin liquid  $\text{Ca}_{10}\text{Cr}_7\text{O}_{28}$ , *Phys. Rev. Mater.* **1**, 024407 (2017).
- [19] See Supplemental Material <http://link.aps.org/supplemental/10.1103/PhysRevB.109.165138> for further information on the calculations reported throughout, which include Refs. [9,11,15,21,26,27].
- [20] S. Sugiura and A. Shimizu, Canonical thermal pure quantum state, *Phys. Rev. Lett.* **111**, 010401 (2013).
- [21] N. Elstner and A. P. Young, Spin-1/2 Heisenberg antiferromagnet on the *kagomé* lattice: High-temperature expansion and exact-diagonalization studies, *Phys. Rev. B* **50**, 6871 (1994).
- [22] H.-J. Schmidt, A. Lohmann, and J. Richter, Eighth-order high-temperature expansion for general Heisenberg Hamiltonians, *Phys. Rev. B* **84**, 104443 (2011).
- [23] A. Lohmann, H.-J. Schmidt, and J. Richter, Tenth-order high-temperature expansion for the susceptibility and the specific heat of spin- $s$  Heisenberg models with arbitrary exchange patterns: Application to pyrochlore and kagome magnets, *Phys. Rev. B* **89**, 014415 (2014).
- [24] S. Blundell, *Magnetism in Condensed Matter* (Oxford University Press, Oxford, UK, 2001).
- [25] J. A. Crossley and C. A. Hooley (unpublished).
- [26] <https://automeris.io/WebPlotDigitizer/>.
- [27] <https://www.wolfram.com/mathematica/>.
- [28] <http://www.uni-magdeburg.de/jschulen/HTE10/>.